Article

The Role of Receptor Uniformity in Multivalent Binding

Xiuyang Xia, Ge Zhang,* Massimo Pica Ciamarra, Yang Jiao, and Ran Ni*

Cite This: *JACS Au* 2023, 3, 1385−1391

Read Online

ACCESS | Metrics & More | Article Recommendations | SI Supporting Information

ABSTRACT: Multivalency is prevalent in various biological systems and applications due to the superselectivity that arises from the cooperativity of multivalent binding. Traditionally, it was thought that weaker individual binding would improve the selectivity in multivalent targeting. Here, using analytical mean field theory and Monte Carlo simulations, we discover that, for receptors that are highly uniformly distributed, the highest selectivity occurs at an intermediate binding energy and can be significantly greater than the weak binding limit. This is caused by an exponential relationship between the bound fraction and receptor concentration, which is influenced by both the strength and combinatorial entropy of binding. Our findings not only provide new guidelines for the rational design of biosensors using multivalent nanoparticles but also introduce a new perspective in understanding biological processes involving multivalency.

KEYWORDS: *multivalent nanoparticle binding, superselectivity, hyperuniformity, combinatorial entropy, Monte Carlo simulation*
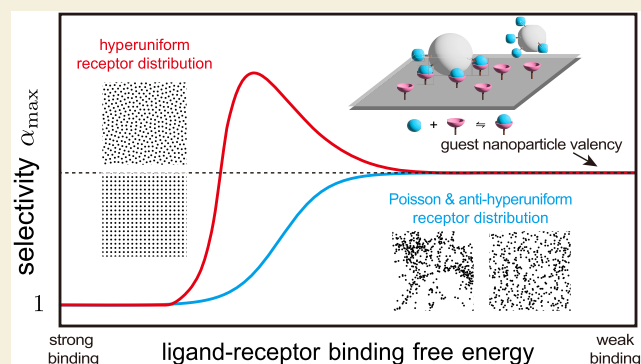
INTRODUCTION

Multivalent interactions play a crucial role in a variety of biological processes.[1−6] They provide an "on−off" binding at a threshold receptor density, creating a biological barcode, targeting surfaces that have a receptor density above the threshold while leaving others untouched. As a result, the multivalent binding strategy is also widely used in many bio-related applications, particularly in drug delivery[7−11] and biosensing.[12−14]

The Martinez-Veracoecha and Frenkel (MF) model provides a selectivity parameter $\alpha = d \ln \theta / d \ln n_R$ quantifying the dependence of targeted adsorption θ on the receptor density n_R.[15] Generally, the maximum of the selectivity parameter α_{max}, where the targeted adsorption grows fastest, is defined as the selectivity employed to characterize the overall selectivity, indicating the onset of guest nanoparticle binding and clustering.[15−17] If the selectivity $\alpha_{max} > 1$, the binding of nanoparticles is superselective, which is a signature of multivalent binding. The MF model predicts that α_{max} increases as the binding strength becomes weaker when neglecting non-specific interactions,[15,18] which was also observed in recent experimental systems including DNA-coated colloids,[19−21] multivalent guest−host polymers,[16,22−24] and influenza virus particles.[25]

All studies mentioned above assume that the receptors grafted on the host substrate follow the Poisson distribution, considering they are random and spatially uncorrelated. However, due to the complex environment on cell membranes, the receptors are heterogeneously distributed and correlated,[26] the effect of which remains unknown. Additionally, recent

breakthroughs in DNA nanotechnology offer the possibility to precisely design the spatial distribution of receptors on a substrate.[27] Here we investigate how the uniformity of receptor distribution affects the selectivity in multivalent nanoparticle binding by focusing on the hyperuniform, Poisson, and anti-hyperuniform distributions.[28] We find that the more uniformly distributed receptors lead to higher selectivity α_{max}, and intriguingly, the maximum selectivity appears at a certain intermediate binding energy for hyperuniform distributions, which is qualitatively different from the Poisson distribution and anti-hyperuniform distributions, with α_{max} approaching the upper bound at the infinitely weak binding energy limit. Moreover, the highest selectivity obtained for receptors of hyperuniform distributions can be significantly larger than the upper bound in the Poisson and anti-hyperuniform distributions, where the relatively large number fluctuation of receptors masks the effect and causes the selectivity to increase monotonically with decreasing binding strength.
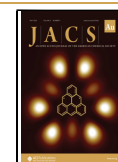
METHODOLOGY

As shown in Figure 1a, we consider that immobile receptors are grafted on a host substrate. The nanoparticles are
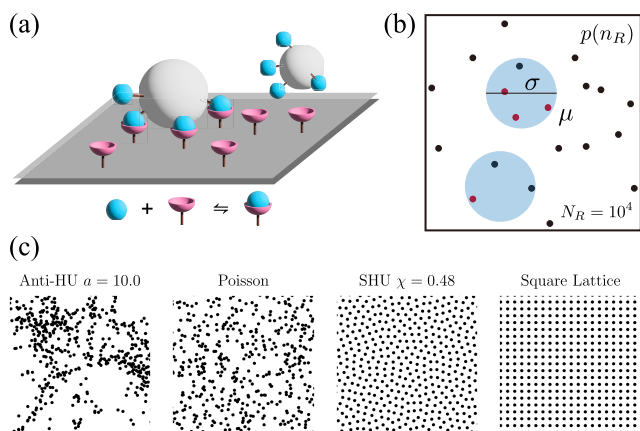
Figure 1. Multivalent nanoparticle binding. (a) Schematic representation of the prototypical multivalent adsorption model, in which the ligands (blue) on the particles (white) can bind with the immobile receptors (pink) on the substrate (gray) reversibly. (b) Illustration of the κ-μVT Monte Carlo simulation, in which some receptors (red) are bound with implicit ligands on the nanoparticles (blue) while the others (black) are unbound. In the simulation, the bonds are implicit. (c) Part of typical snapshots of receptors following various distributions. The global typical snapshots of receptors can be found in the SI.

controlled by an activity $z = v_0 \exp(\beta\mu)$, with μ the chemical potential of nanoparticles and $\beta = 1/k_B T$, where v_0 is the volume that each particle can explore when bound on the substrate, and k_B and T are the Boltzmann constant and temperature of the system, respectively. Each nanoparticle is coated with κ mobile ligands, which can bind to the receptors reversibly with the binding free energy f_B. The binding free energy f_B is determined by both the equilibrium constant of ligand–receptor binding in solvent K_a and the configurational entropy penalty due to the constraint of tethering ΔS_{conf}: $\beta f_B = -\log K_a - k_B^{-1}\Delta S_{conf}$.[29] Assuming that the adsorption of each guest particle is independent, we divide the substrate into N_{max} sites, each of which can bind with one guest particle at most. The fraction of sites that are occupied by particles with at least one bond formed is

$$\theta(z, n_R) = \frac{zq(n_R)}{1 + zq(n_R)} \tag{1}$$

Using the unbound site as the reference state, the single-site bound state partition function $q(n_R)$ with n_R receptors can be written as

$$q(n_R) = \sum_{\lambda=1}^{\min(\kappa, n_R)} Q(\lambda, n_R) \tag{2}$$

where λ is the number of bonds formed and

$$Q(\lambda, n_R) = e^{-\lambda \beta f_B} \frac{\kappa! n_R!}{(\kappa - \lambda)! \lambda! (n_R - \lambda)!} \tag{3}$$

Then the fraction of bound sites or adsorption is

$$\langle\theta\rangle = \left\langle \frac{zq}{1 + zq} \right\rangle_{\langle n_R \rangle} \tag{4}$$

where $\langle\cdot\rangle_{\langle n_R \rangle}$ calculates the average over the receptor number distribution with the mathematical estimate $\langle n_R \rangle$. The selectivity parameter is defined as

$$\alpha = \frac{d \ln \langle\theta\rangle}{d \ln \langle n_R \rangle} \tag{5}$$

Since the higher selectivity usually appears at small activity,[15,30,31] the time for the substrate to exchange nanoparticles with the reservoir to reach equilibrium is very long, which makes the direct Monte Carlo (MC) simulations in 3D systems expensive and inefficient. Here we propose a κ-μVT MC simulation method with implicit ligands and bonds in 2D, which enables us to efficiently sample in the additional bond number dimension (see simulation methods in the Supporting Information (SI)). As shown in Figure 1b, we model the multivalent nanoparticles as hard disks of diameter σ and volume $s_{hd} = \pi\sigma^2/4$ controlled by the chemical potential μ. We assume that one receptor can only bind with the particle covering it; i.e., the center-to-center distance between the receptor and ligand is less than $\sigma/2$. The total number of sites $N_{max} = L^2/s_{hd}$, and the average number of receptors per site $\langle n_R \rangle = N_R s_{hd}/L^2$. The activity $z = s_{hd} \exp(\beta\mu)/\Lambda^2$, with Λ the de Broglie wavelength. The distribution $p(n_R)$ is numerically sampled by the number of receptors within a 2D spherical window of radius $\sigma/2$. One can see that the κ-μVT MC simulation essentially simulates a monolayer of nanoparticles near the host substrate, where nanoparticles can bind with receptors on the substrate, and the system exchanges nanoparticles with a bulk (3D) reservoir of chemical potential μ above. The advantage of the κ-μVT model is that one does not need to explicitly simulate the exchange of nanoparticles between the host substrate and bulk reservoir through diffusion, which could be very computationally expensive at small activity.

■ RESULTS

Receptor Uniformity Enhances Selectivity

We consider four different types of receptor distributions: anti-hyperuniform (Anti-HU) distributions,[32] the Poisson distribution, stealthy hyperuniform (SHU) distributions[33,34] and a square lattice (Figure S1). In equilibrium, Anti-HU can describe systems close to a critical point, and SHU describes the disordered systems with long-range correlations.[32] All those distributions are statistically homogeneous point processes and follow the central limit theorem, i.e., they can be approximated by Gaussian distributions at the large $\langle n_R \rangle$ limit.[28] The spatial uniformity of a receptor distribution at given $\langle n_R \rangle$ can be characterized by the relative local number variance $\sigma_{n_R}^2/\langle n_R \rangle$. For the Poisson distribution in 2D, $\sigma_{n_R}^2/\langle n_R \rangle = 1$. For a perfect square lattice, $\sigma_{n_R}^2/\langle n_R \rangle \sim \langle n_R \rangle^{-1/2}$, which essentially implies that the square lattice is more uniform than the Poisson distribution.

SHU distributions follow the same scaling with the square lattice. The configurations are generated by minimizing $\Phi(\mathbf{r}^N) = \sum_{|\mathbf{k}|<K} S(\mathbf{k})$ using the limited-memory BFGS algorithm,[35] starting from a Poisson configuration with number density $\rho = 1$. Here $K = 4\sqrt{\pi\chi}$[34] and $\chi = M(K)/[D(N_R - 1)]$ denotes the relative fraction of constrained degrees of freedom compared to the total degrees of freedom $D(N_R - 1)$ with $M(K)$ the number of independently constrained wave vectors.[32] The prefactor of the distributions depends on the parameter χ with the larger χ being more uniform or with smaller density fluctuations.

On the contrary, in Anti-HU structures, $\sigma_{n_R}^2$ increases faster than $\langle n_R \rangle$, and here we choose configurations that exhibit $\sigma_{n_R}^2 / \langle n_R \rangle \sim \langle n_R \rangle^{1/2}$. The Anti-HU configurations are generated using the algorithm detailed in ref 36. Specifically, we use the limited-memory BFGS algorithm to minimize $\sum_{|\mathbf{k}|<K}[\langle S(\mathbf{k}) \rangle - S_0(\mathbf{k})]^2$, in which $K = 10$, $\langle S(\mathbf{k}) \rangle$ is the average structure factor $S(\mathbf{k}) = |\sum_{j=1}^{N_R} \exp(-i\mathbf{k} \cdot \mathbf{r}_j)|^2 / N$ over $N_c = 100$ configurations, and the targeted structure factor for various a is $S_0(\mathbf{k}) = 1 + a \exp(-|\mathbf{k}|)/|\mathbf{k}|$. The prefactor of the distributions depends on the parameter a, with the larger a being less uniform or with the larger density fluctuations. For each structure, we individually generate 10 snapshots of 10^4 receptors to sample the spatial distribution and to be used in MC simulations.

In Figure 2, we plot the average bound fraction $\langle \theta \rangle$ and the selectivity parameter α as functions of $\langle n_R \rangle$ for various receptor
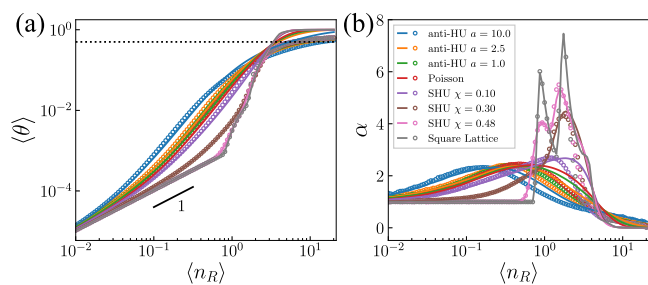

Figure 2. Receptor uniformity enhances selectivity. Average bound fraction $\langle \theta \rangle$ (a) and selectivity parameter α (b) as a function of $\langle n_R \rangle$ with $\kappa = 4$, $\beta f_B = -2$, and $\beta \mu = -10$ for various receptors distributions. The solid curves are the theoretical predictions of eqs 4 and 5, and the symbols are obtained from simulations.

distributions. One can see that eqs 4 and 5 agree quantitatively with computer simulations when $\langle \theta \rangle < 0.5$ (indicated by the dotted horizontal line), and at very large $\langle n_R \rangle$, the theoretically predicted $\langle \theta \rangle$ is larger. This discrepancy is due to the fact that the excluded volume effect between nanoparticles is not considered in the mean field theory, which overestimates the

adsorption at high density. When $\langle n_R \rangle$ is small, with increasing $\langle n_R \rangle$, less uniform distributions lead to larger value of $\langle \theta \rangle$. This is because that $\langle \theta \rangle \approx z \langle q \rangle$ according to eq 4, where the average bound state partition function over the receptor distribution $\langle q \rangle$ is a convex function (see SI); hence, $\langle q \rangle$ increases with increasing the variance of the distribution $\sigma_{n_R}^2$. As shown in Figure 2, with increasing the uniformity, i.e., from Anti-HU to the Poisson, SHU structures, and square lattice, the selectivity α_{max} increases monotonically, and for SHU structures and square lattice, α_{max} is even larger than $\kappa = 4$. This is intriguing as it has been accepted that weaker binding energy enhances selectivity, of which the upper bound of α_{max} is κ.[15]

Achieving the Highest Selectivity by Tuning Binding Energy

In Figure 3, we plot $\langle \theta \rangle$ and α as functions of $\langle n_R \rangle$ for binding energy from strong ($\beta f_B = -6$) to weak ($\beta f_B = 4$) of various receptor distributions. For the receptor structures of the Poisson and Anti-HU distributions, α_{max} increases monotonically with increasing βf_B, namely weaker binding enhances selectivity, while for SHU structures with $\chi = 0.48$ and square lattice, α_{max} reaches the maximum at about $\beta f_B = -4$. To understand this, we start with the selectivity parameter $\alpha_{zv} = $ d ln θ/d ln n_R in the zero variance scenario, which is the uniform limit of receptors with $\sigma_{n_R}^2 = 0$. As the superselective adsorption of nanoparticles of interest mostly occurs at low activity, according to eq 1, when $zq \to 0$, $\theta(n_R) \approx zq(n_R)$ and $\alpha_{zv} \approx $ d ln q/d ln n_R. We define the selectivity parameter at the low activity limit as $\alpha_{zv,0} = $ d ln q/d ln n_R.[37] We plot the probability of forming λ bonds on the guest nanoparticle in the bound state in Figure 4a. For weak binding $\beta f_B = 4$ and small n_R, one can see $q(n_R) \approx Q(\langle \lambda \rangle_{bound}, n_R)$, with the most probable bond number $\langle \lambda \rangle_{bound} \approx 1$ (yellow region in upper panel of Figure 4a). This implies that there is only one bond formed for the particle bound on the substrate, and the ligands on each particle cannot bind cooperatively. As shown in Figure 4b, this leads to a linear dependence $q \approx n_R \kappa$ e$^{-\beta f_B}$ and $\alpha_{zv,0} \approx 1$ with no superselectivity. With increasing n_R, $\langle \lambda \rangle_{bound}$ approaches κ at the large n_R limit due to the restriction from the number of
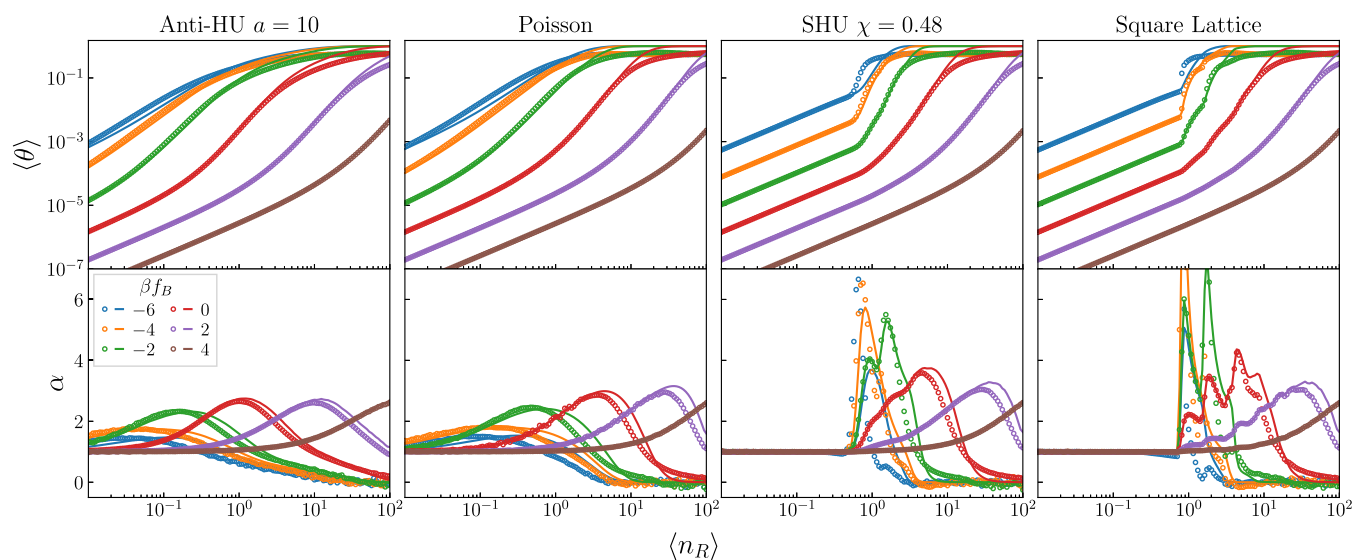

Figure 3. Achieving the highest selectivity by tuning binding free energy. $\langle \theta \rangle$ and α as a function of $\langle n_R \rangle$ for various binding free energy βf_B for typical receptors structures: Anti-HU $a = 10$, Poisson, SHU $\chi = 0.48$, and square lattice. The solid curves are the theoretical predictions of eqs 4 and 5, and the symbols are obtained from simulations. In all simulations, $\kappa = 4$ and $\beta \mu = -10$.
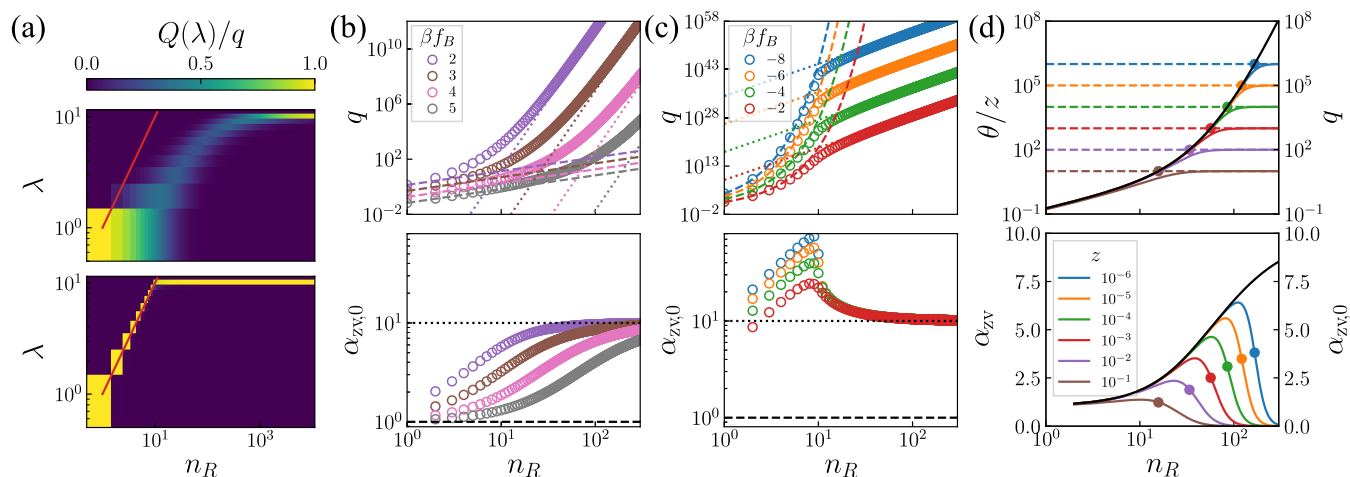
Figure 4. Multivalent binding of nanoparticles in the zero variance scenario. (a) The probability for λ bonds formed on bound guest nanoparticles $Q(\lambda)/q$ as a function of n_R for $\beta f_B = 4$ (upper) and -4 (lower). (b, c) The zero variance bound state partition function q and zero variance selectivity at low activity limit $\alpha_{zv,0}$ as a function of n_R. Open symbols are the analytical results from eq 2. Colored dotted lines are from eq 6. Colored dashed lines are (b) $q = n_R e^{-\beta f_B}$ and (c) eq 7, respectively. Black dashed and dotted lines indicate $\alpha_{zv,0} = 1$ and κ, respectively. (d) θ/z (upper colored solid curves), q (upper black curve), α_{zv} (lower colored curves), and $\alpha_{zv,0}$ (lower black curve) as a function of n_R with $\beta f_B = 4$ for various activity z. Symbols indicate the position of n_R^s, which is the crosspoint of θ/z and $1/z$ (upper colored dashed curves). In all calculations, $\kappa = 10$.

ligands available on nanoparticles, and this leads to a power-law dependence of q on n_R (see SI):

$$q \approx Q(\lambda = \kappa, n_R) = e^{-\kappa \beta f_B} \frac{n_R!}{(n_R - \kappa)!} \approx (n_R \, e^{-\beta f_B})^\kappa \tag{6}$$

and $\alpha_{zv,0} \approx \kappa$. Here, κ ligands on each particle bind with crowded receptors together, and the emergent combinatorial entropy induces the power-law dependence.

Differently, at the strong binding $\beta f_B = -4$, although the power-law dependence also appears at the large n_R limit, in the small n_R regime, i.e., $1 < n_R < \kappa$, as shown in the lower panel in Figure 4a, the most probable bond number $\langle \lambda \rangle_{bound} \approx n_R$. It is because that the most probable bond number is limited by the number of receptors on each site of the host substrate, rather than the number of ligands on the nanoparticles, which implies an exponential dependence of q on n_R (see SI):

$$q \approx Q(\lambda = n_R, n_R) = e^{-n_R \beta f_B} \frac{\kappa!}{(\kappa - n_R)!} \approx (\kappa \, e^{-\beta f_B})^{n_R} \tag{7}$$

and $\alpha_{zv,0} \approx n_R(\ln \kappa - \beta f_B) \sim n_R$. These are the major results of this work. The derivation of eqs 6 and 7 based on the saddle-point approximation method[17,38,39] can be found in the SI. As shown in Figure 4c, $\alpha_{zv,0}$ peaks around $n_R = \kappa$, which is independent of the binding energy, and the selectivity $\alpha_{zv,0}^{max} \approx \kappa(\ln \kappa - \beta f_B)$ can be larger than κ when $\beta f_B < \ln \kappa - 1$. Hence, in the zero variance binding scenario, $\ln \kappa - 1$ is a threshold of binding energy, lower than which $\alpha_{zv,0}^{max} > \kappa$, otherwise $\alpha_{zv,0}^{max}$ has an upper bound κ at $n_R \to +\infty$.

As shown in Figure 4d, the rescaled bound fractions θ/z at various activity z collapse at small n_R, while they reach plateaus of different heights at high n_R. The behavior is qualitatively the same when considering receptor distributions (Figure S3). This indicates that z does not affect the selectivity parameter when $n_R < n_R^s$, where $q(n_R^s) \approx 1/z$ is the bound fraction saturation threshold. Therefore, the zero variance selectivity parameter $\alpha_{zv} \approx \alpha_{zv,0}$ at n_R is lower than the threshold, and drops to 0 with further increasing n_R. Moreover, when $zq(n_R =$

1) > 1, i.e., $\beta f_B < \ln(z\kappa)$, the bound fraction saturates even if only one nanoparticle binds to one receptor, and no superselectivity occurs. To sum up, an exponential dependence occurs at $\ln(z\kappa) < \beta f_B < \ln \kappa - 1$ and $1 < n_R < \kappa$ in the zero variance scenario.

For the highly uniformly distributed receptors, e.g., SHU $\chi = 0.48$ and the square lattice in Figure 3, the situation is qualitatively the same to the zero variance scenario since the variance of the receptor distribution is small. The largest α_{max} occurs at an intermediate binding energy with a larger value than κ. Additionally, the critical $\langle n_R \rangle$ with α_{max} appears independent of the binding energy $\beta f_B = -6$ and -4, which is a distinct feature of the exponential dependence.

For the Poisson and less uniform receptor distributions, i.e., Anti-HU, our numerical evidence shows that α_{max} increases monotonically with increasing βf_B and approaches κ at $\beta f_B \to +\infty$ (Figure 3). We believe that this is due to the relatively large receptor number fluctuations masking the exponential dependence in the intermediate binding energy. As shown in Figure S4, in the weak binding limit, receptor uniformity has little effect on $\langle \theta \rangle$, and $\alpha_{max} \to \kappa$ holds as long as the receptor distribution obeys the central limit theorem and satisfies $\sigma_{n_R}^2 < \langle n_R \rangle^2$ at large $\langle n_R \rangle$ (see SI). Therefore, weaker binding enhances the selectivity with an upper bound limit κ for those less uniform distributions.[15]

Next we investigate the binding of multivalent nanoparticles to receptors with tunable local uniformity. We use the configurations of receptors obtained from equilibrium fluids of hard disks (HD) of various packing fraction ϕ. When $\phi \to 0$, the HD system recovers an ideal gas of the Poisson distribution, i.e., $\sigma_{n_R}^2/\langle n_R \rangle = 1$, and with increasing ϕ, at certain length scale, $\sigma_{n_R}^2/\langle n_R \rangle \sim \langle n_R \rangle^\xi$, with $\xi < 0$, which is the local uniformity induced by the increased short-range correlation because of the excluded volume effect (Figure S5). The local uniformity of the configuration increases with increasing ϕ of HD systems, while at large enough length scale $\sigma_{n_R}^2/\langle n_R \rangle \sim \langle n_R \rangle^0$ (Figure S5). The measured α_{max} as functions

of binding strength βf_B for different ϕ are shown in Figure 5. One can see that, with small local uniformity, e.g., $\phi = 0.01$,
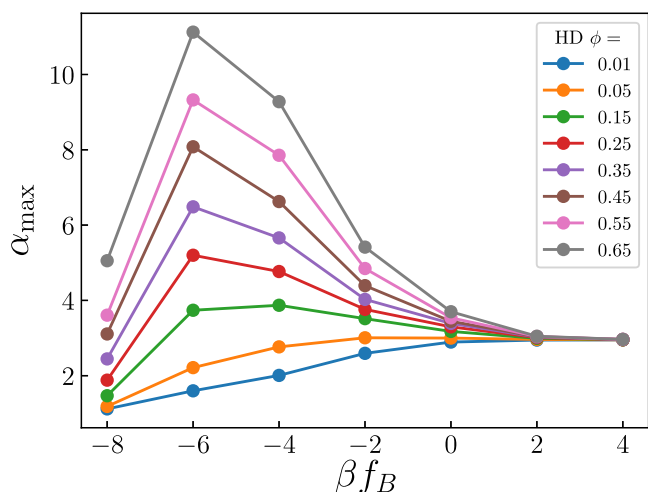

Figure 5. Superselectivity of multivalent nanoparticle binding on receptors of tunable local uniformity. Selectivity α_{max} as a function of binding strength βf_B for structures obtained from equilibrium hard-disk fluids at various packing fraction ϕ. In all simulations, $\kappa = 4$ and $\beta\mu = -10$.

α_{max} increases monotonically with increasing βf_B, which is the same as receptors of the Poisson distribution (Figure S6). However, with increasing ϕ, the non-monotonic dependence of α_{max} on βf_B appears when $\phi > 0.15$ (Figure S6). This implies that the local uniformity induced by the excluded volume effect can trigger the non-monotonic dependence of selectivity on the binding free energy.

Here we consider the binding of multivalent nanoparticles on a rigid flat substrate, while on a cell membrane, as more bonds form with the nanoparticles, the membrane roughness decreases. Because the bonds suppress membrane shape fluctuations, which promotes the formation of additional bonds cooperatively.[40,41] In our model, we can consider the thermal roughness of flexible substrates by rewriting the partition function of λ bonds forming in eq 3 to include an entropy cost, $\Delta S_{mem}(\lambda)$, that originates from the suppression of membrane shape fluctuations upon λ bonds formation. This term depends on the relative roughness of the membranes, $\xi_\perp \sim \lambda^{1/2}$, and a characteristic length ξ_{RL} that represents the extension of the receptor−ligand complex perpendicular to the membranes.[42] When $\xi_\perp \gg \xi_{RL}$, we have $e^{k_B^{-1}\Delta S_{mem(\lambda)}} \sim \xi_\perp^{-1} \sim \lambda^{0.5}$.[43] At the large n_R limit, where $q \approx Q(\lambda = \kappa, n_R)$, the entropy cost term ΔS_{mem} is a constant because of the constant number of bonds, and eq 6 remains valid. At this limit, the suppression of membrane shape fluctuation has no qualitative effect on $\alpha_{zv,0}$. However, an additional term should be added to $\alpha_{zv,0}$ to account for the contribution of ΔS_{mem}. This term is $d \log e^{k_B^{-1}\Delta S_{mem(n_R)}}/d \log n_R$, which is round 0.5 at the strong binding limit when $1 < n_R \ll \kappa$. This suggests that the suppression of membrane shape fluctuations can enhance the superselectivity.

■ **DISCUSSION**

In conclusion, we have investigated the impact of receptor uniformity on the superselective binding of multivalent nanoparticles, for which we devised a κ-μVT MC simulation

method to compare with the analytical theory without any fitting parameter. We find that receptors that are more uniformly distributed lead to stronger superselective binding of multivalent particles. Specifically, for receptors with SHU structures and square lattice arrangements, the selectivity, α_{max}, can be significantly larger than the valence of the nanoparticle, κ, which is the highest level of selectivity that receptors with Poisson and Anti-HU distributions can achieve. Furthermore, for receptors with SHU distributions and square lattice arrangements, the largest α_{max} occurs at an intermediate strength of binding energy, which is due to the exponential dependence of the bound fraction on the receptor density. The exponential dependence arises from the restriction of available receptors and is affected by both the binding energy and combinatorial entropy. This is different from the binding on receptors with Poisson or Anti-HU distributions, where weaker binding always enhances the selectivity. These results suggest that, for receptors that are highly uniformly distributed, one does not have to use very weak binding energy to achieve high selectivity, and the largest α_{max} occurs at a certain relatively strong binding that is less affected by non-specific attraction.

Our findings are relevant for designing superselective sensors using multivalent nanoparticles, a possible design of which is shown in Figure 6. Based on our results, one can use arrays of
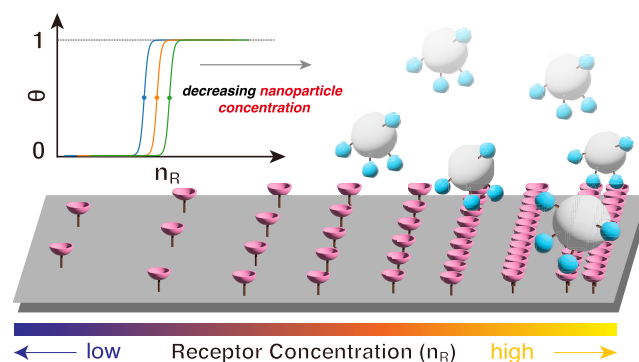

Figure 6. Possible design of a superselective sensor for multivalent nanoparticles. The design consists of arrays of orderly arranged receptors of density n_R increasing from left to right, which can be realized by using DNA origami.[27] The inset shows typical adsorption curves θ of multivalent nanoparticles on the bands of receptors of different n_R grafted on the substrate.

orderly arranged receptors of different density using DNA origami to enhance the superselectivity using strongly binding multivalent nanoparticles to avoid the influence of non-specific attraction.[27] This also suggests the possibility of designing superselective assembly of receptor-patterned colloidal systems.[44,45] Additionally, our findings emphasize the significance of receptor distribution in biological systems. Although in principle many receptors on cell membranes are mobile, the receptor diffusion time scale on cell membranes, t_{diff}, could be much longer than the time it takes to form/break a bond with ligands on nanoparticles, $t_{on/off}$. This suggests that these receptors can be considered as effectively immobile. Furthermore, there are also many immobile receptors on cell membranes that are restricted and compartmentalized due to interactions with the cytoskeleton.[46] Moreover, we also show that the local uniformity induced by excluded volume effects can trigger the non-monotonic dependence of selectivity on the binding free energy, which suggests that our finding can be

expected in systems of relatively densely packed receptors, like the situation in many biological membranes.

ASSOCIATED CONTENT

Supporting Information

The Supporting Information is available free of charge at https://pubs.acs.org/doi/10.1021/jacsau.3c00052.

Simulation methods, additional theory details, and Figures S1–S6 (PDF)

AUTHOR INFORMATION

Corresponding Authors

Ge Zhang − *Department of Physics, City University of Hong Kong, 518057 Kowloon, Hong Kong, China;* Email: gzhang37@cityu.edu.hk

Ran Ni − *School of Chemistry, Chemical Engineering and Biotechnology, Nanyang Technological University, 637459, Singapore;* orcid.org/0000-0001-9478-0674; Email: r.ni@ntu.edu.sg

Authors

Xiuyang Xia − *School of Chemistry, Chemical Engineering and Biotechnology, Nanyang Technological University, 637459, Singapore; Division of Physics and Applied Physics, School of Physical and Mathematical Sciences, Nanyang Technological University, 637371, Singapore;* orcid.org/0000-0002-4851-4057

Massimo Pica Ciamarra − *Division of Physics and Applied Physics, School of Physical and Mathematical Sciences, Nanyang Technological University, 637371, Singapore;* orcid.org/0000-0001-8931-9058

Yang Jiao − *Materials Science and Engineering, Arizona State University, Tempe, Arizona 85287, United States*

Complete contact information is available at: https://pubs.acs.org/10.1021/jacsau.3c00052

Notes

The authors declare no competing financial interest.

ACKNOWLEDGMENTS

REFERENCES

(1) Mammen, M.; Choi, S.-K.; Whitesides, G. M. Polyvalent interactions in biological systems: implications for design and use of multivalent ligands and inhibitors. *Angew. Chem., Int. Ed.* **1998**, *37*, 2754−2794.

(2) Boudreau, N. J.; Jones, P. L. Extracellular matrix and integrin signalling: the shape of things to come. *Biochem. J.* **1999**, *339*, 481−488.

(3) Huskens, J. Multivalent interactions at interfaces. *Curr. Opin. Chem. Biol.* **2006**, *10*, 537−543.

(4) Fasting, C.; Schalley, C. A.; Weber, M.; Seitz, O.; Hecht, S.; Koksch, B.; Dernedde, J.; Graf, C.; Knapp, E.-W.; Haag, R. Multivalency as a chemical organization and action principle. *Angew. Chem., Int. Ed.* **2012**, *51*, 10472−10498.

(5) Satav, T.; Huskens, J.; Jonkheijm, P. Effects of variations in ligand density on cell signaling. *Small* **2015**, *11*, 5184−5199.

(6) Karimi, F.; O'Connor, A. J.; Qiao, G. G.; Heath, D. E. Integrin clustering matters: a review of biomaterials functionalized with multivalent integrin-binding ligands to improve cell adhesion, migration, differentiation, angiogenesis, and biomedical device integration. *Adv. Healthcare Mater.* **2018**, *7*, 1701324.

(7) Baker, M. Homing in on delivery. *Nature* **2010**, *464*, 1225−1227.

(8) Bartlett, D. W.; Su, H.; Hildebrandt, I. J.; Weber, W. A.; Davis, M. E. Impact of tumor-specific targeting on the biodistribution and efficacy of sirna nanoparticles measured by multimodality in vivo imaging. *Proc. Natl. Acad. Sci. U. S. A.* **2007**, *104*, 15549−15554.

(9) Davis, M. E.; Zuckerman, J. E.; Choi, C. H. J.; Seligson, D.; Tolcher, A.; Alabi, C. A.; Yen, Y.; Heidel, J. D.; Ribas, A. Evidence of rnai in humans from systemically administered sirna via targeted nanoparticles. *Nature* **2010**, *464*, 1067−1070.

(10) Akhtar, M. J.; Ahamed, M.; Alhadlaq, H. A.; Alrokayan, S. A.; Kumar, S. Targeted anticancer therapy: overexpressed receptors and nanotechnology. *Clinica chimica acta* **2014**, *436*, 78−92.

(11) Koenig, P.-A.; Das, H.; Liu, H.; Kümmerer, B. M.; Gohr, F. N.; Jenster, L.-M.; Schiffelers, L. D. J.; Tesfamariam, Y. M.; Uchima, M.; Wuerth, J. D.; et al. Structure-guided multivalent nanobodies block sars-cov-2 infection and suppress mutational escape. *Science* **2021**, *371*, eabe6230.

(12) Zeng, X.; Andrade, C. A. S.; Oliveira, M. D. L.; Sun, X.-L. Carbohydrate-protein interactions and their biosensing applications. *Anal. Bioanal. Chem.* **2012**, *402*, 3161−3176.

(13) Zhou, G.; Lin, M.; Song, P.; Chen, X.; Chao, J.; Wang, L.; Huang, Q.; Huang, W.; Fan, C.; Zuo, X. Multivalent capture and detection of cancer cells with dna nanostructured biosensors and multibranched hybridization chain reaction amplification. *Analytical chemistry* **2014**, *86*, 7843−7848.

(14) Cai, W. *Engineering in translational medicine*; Springer, 2014.

(15) Martinez-Veracoechea, F. J.; Frenkel, D. Designing super selectivity in multivalent nano-particle binding. *Proc. Natl. Acad. Sci. U. S. A.* **2011**, *108*, 10963−10968.

(16) Albertazzi, L.; Martinez-Veracoechea, F. J.; Leenders, C. M. A.; Voets, I. K.; Frenkel, D.; Meijer, E. W. Spatiotemporal control and superselectivity in supramolecular polymers using multivalency. *Proc. Natl. Acad. Sci. U. S. A.* **2013**, *110*, 12203−12208.

(17) Angioletti-Uberti, S. Exploiting receptor competition to enhance nanoparticle binding selectivity. *Phys. Rev. Lett.* **2017**, *118*, 068001.

(18) Curk, T.; Dobnikar, J.; Frenkel, D. Optimal multivalent targeting of membranes with many distinct receptors. *Proc. Natl. Acad. Sci. U. S. A.* **2017**, *114*, 7210−7215.

(19) Scheepers, M. R. W.; van IJzendoorn, L. J.; Prins, M. W. J. Multivalent weak interactions enhance selectivity of interparticle binding. *Proc. Natl. Acad. Sci. U. S. A.* **2020**, *117*, 22690−22697.

(20) Linne, C.; Visco, D.; Angioletti-Uberti, S.; Laan, L.; Kraft, D. J. Direct visualization of superselective colloid-surface binding mediated by multivalent interactions. *Proc. Natl. Acad. Sci. U. S. A.* **2021**, *118*, e2106036118.

(21) Zhang, Y.; He, X.; Zhuo, R.; Sha, R.; Brujic, J.; Seeman, N.; Chaikin, P. Multivalent, multiflavored droplets by design. *Proc. Natl. Acad. Sci. USA* **2018**, *115*, 9086−9091.

(22) Dubacheva, G. V.; Curk, T.; Mognetti, B. M.; Auzély-Velty, R.; Frenkel, D.; Richter, R. P. Superselective targeting using multivalent polymers. *J. Am. Chem. Soc.* **2014**, *136*, 1722−1725.

(23) Dubacheva, G. V.; Curk, T.; Auzély-Velty, R.; Frenkel, D.; Richter, R. P. Designing multivalent probes for tunable superselective targeting. *Proc. Natl. Acad. Sci. U. S. A.* **2015**, *112*, 5579−5584.

(24) Dubacheva, G. V.; Curk, T.; Frenkel, D.; Richter, R. P. Multivalent recognition at fluid surfaces: The interplay of receptor clustering and superselectivity. *J. Am. Chem. Soc.* **2019**, *141*, 2577−2588.

(25) Overeem, N. J.; Hamming, P. H. E.; Grant, O. C.; Di Iorio, D.; Tieke, M.; Bertolino, M. C.; Li, Z.; Vos, G.; De Vries, R. P.; Woods, R. J.; et al. Hierarchical multivalent effects control influenza host specificity. *ACS Central Science* **2020**, *6*, 2311−2318.

(26) Lingwood, D.; Simons, K. Lipid rafts as a membrane-organizing principle. *Science* **2010**, *327*, 46−50.

(27) Bila, H.; Paloja, K.; Caroprese, V.; Kononenko, A.; Bastings, M. Multivalent pattern recognition through control of nano-spacing in low-valency super-selective materials. *J. Am. Chem. Soc.* **2022**, *144*, 21576.

(28) Torquato, S.; Kim, J.; Klatt, M. A. Local number fluctuations in hyperuniform and nonhyperuniform systems: Higher-order moments and distribution functions. *Physical Review X* **2021**, *11*, 021028.

(29) Leunissen, M. E.; Dreyfus, R.; Sha, R.; Seeman, N. C.; Chaikin, P. M. Quantitative study of the association thermodynamics and kinetics of dna-coated particles for different functionalization schemes. *J. Am. Chem. Soc.* **2010**, *132*, 1903−1913.

(30) Wang, S.; Dormidontova, E. E. Selectivity of ligand-receptor interactions between nanoparticle and cell surfaces. *Physical Review Letters* **2012**, *109*, 238102.

(31) Phan, H. T.; Lauzon, D.; Vallee-Belisle, A.; Angioletti-Uberti, S.; Leblond Chain, J.; Giasson, S. Bimodal brush-functionalized nanoparticles selective to receptor surface density. *Proc. Natl. Acad. Sci. U. S. A.* **2023**, *120*, e2208377120.

(32) Torquato, S. Hyperuniform states of matter. *Phys. Rep.* **2018**, *745*, 1−95.

(33) Florescu, M.; Torquato, S.; Steinhardt, P. J. Designer disordered materials with large, complete photonic band gaps. *Proc. Natl. Acad. Sci. U. S. A.* **2009**, *106*, 20658−20663.

(34) Torquato, S.; Zhang, G.; Stillinger, F. H. Ensemble theory for stealthy hyperuniform disordered ground states. *Physical Review X* **2015**, *5*, 021020.

(35) Liu, D. C.; Nocedal, J. On the limited memory bfgs method for large scale optimization. *Mathematical Programming* **1989**, *45*, 503−528.

(36) Torquato, S. Structural characterization of many-particle systems on approach to hyperuniform states. *Phys. Rev. E* **2021**, *103*, 052126.

(37) Numerically, we calculate the zero variance selectivity using the finite difference of q or θ in the log-log scale: $\alpha_{zv} = [\log \theta(n_R + 1) - \log \theta(n_R - 1)]/\log(n_R + 1) - \log(n_R - 1)]$ and $\alpha_{zv,0} = [\log q(n_R + 1) - \log q(n_R - 1)]/[\log(n_R + 1) - \log(n_R - 1)]$, respectively.

(38) Varilly, P.; Angioletti-Uberti, S.; Mognetti, B. M.; Frenkel, D. A general theory of dna-mediated and other valence-limited colloidal interactions. *J. Chem. Phys.* **2012**, *137*, 094108.

(39) Angioletti-Uberti, S.; Varilly, P.; Mognetti, B. M.; Tkachenko, A. V.; Frenkel, D. Communication: A simple analytical formula for the free energy of ligand-receptor-mediated interactions. *J. Chem. Phys.* **2013**, *138*, 021102.

(40) Krobath, H.; Rozycki, B.; Lipowsky, R.; Weikl, T. R. Binding cooperativity of membrane adhesion receptors. *Soft Matter* **2009**, *5*, 3354−3361.

(41) Steinkühler, J.; Różycki, B.; Alvey, C.; Lipowsky, R.; Weikl, T. R.; Dimova, R.; Discher, D. E Membrane fluctuations and acidosis regulate cooperative binding of 'marker of self' protein cd47 with the macrophage checkpoint receptor sirpα. *Journal of Cell Science* **2018**, *132*, jcs216770.

(42) Hu, J.; Lipowsky, R.; Weikl, T. R. Binding constants of membrane-anchored receptors and ligands depend strongly on the nanoscale roughness of membranes. *Proc. Natl. Acad. Sci. U. S. A.* **2013**, *110*, 15283−15288.

(43) Krobath, H.; Schutz, G. J.; Lipowsky, R.; Weikl, T. R. Lateral diffusion of receptor-ligand bonds in membrane adhesion zones: Effect of thermal membrane roughness. *Europhys. Lett.* **2007**, *78*, 38003.

(44) Mognetti, B. M.; Cicuta, P.; Di Michele, L. Programmable interactions with biomimetic dna linkers at fluid membranes and interfaces. *Rep. Prog. Phys.* **2019**, *82*, 116601.

(45) Song, J.; Rizvi, M. H.; Lynch, B. B.; Ilavsky, J.; Mankus, D.; Tracy, J. B.; McKinley, G. H.; Holten-Andersen, N. Programmable anisotropy and percolation in supramolecular patchy particle gels. *ACS Nano* **2020**, *14*, 17018−17027.

(46) Choquet, D.; Triller, A. The role of receptor diffusion in the organization of the postsynaptic membrane. *Nat. Rev. Neurosci.* **2003**, *4*, 251−265.